

Mobile robot path tracking of aggressive maneuvers on sloped terrain

Steven C. Peters and Karl Iagnemma

Abstract—Path tracking control on non-flat terrain is an important capability of mobile robots operating in outdoor environments. A path tracking controller based on the model predictive control (MPC) framework is presented that explicitly considers terrain geometry and actuator limitations. The controller performance is studied with three vehicle dynamic models in a high-fidelity ADAMS simulation. The effect of model order on path tracking performance on flat terrain and sloped terrain is evaluated. It is shown that improved performance can be obtained by explicitly considering terrain effects.

I. INTRODUCTION

AUTONOMOUS navigation of mobile robots on rugged terrain at high speeds has received substantial research attention recently, as highlighted by the DARPA Grand Challenge competition [1]. Applications of high speed mobile robots include exploration, military reconnaissance, and material transport. In these scenarios, increasing vehicle speed may reduce danger to the vehicle and improve task efficiency. Research for safe autonomous operation of mobile robots on rugged terrain can also be applied to improve the safety of human-operated vehicles, which cause more than \$200 billion in damage and 40,000 deaths annually in the United States alone [2].

High speed mobile robot navigation systems require a number of capabilities for successful operation, including environment sensing, rapid vehicle path planning, and robust control of the vehicle along the desired path. This paper considers the problem of path tracking through an environment with sloped terrain. Three major challenges of path tracking on sloped terrain include the dynamics of tire and suspension compliance during aggressive maneuvers, the effect of limited actuation, and the effect of terrain slope on path tracking performance and vehicle rollover stability.

Numerous path tracking controllers have been developed for mobile robots operating in a plane with no-slip constraints [3-5]. Wheel slip does occur in practice, however, particularly as a result of tire compliance during aggressive maneuvers at high speed [6-7].

Nonlinear models of tire compliance have been validated in aggressive maneuvers with lateral acceleration greater than 0.5 g [6]. Linearization of these models is considered

valid up to 0.3 g of lateral acceleration [7]. Several path-tracking controllers utilize this model of wheel slip. A path tracking controller for autonomous highways used frequency-shaped linear quadratic control with preview of upcoming road curvature and inclination. This controller was shown to closely track trajectories with lateral acceleration of 0.15 g [8]. Optimal control was used to evaluate the effectiveness of several vehicle actuator configurations in emergency lane change maneuvers, including steer-by-wire, differential braking, and active suspension [9]. The controller demonstrated close tracking for lateral accelerations of 0.3 g.

Model predictive control (MPC), a general control framework for control of systems with hard constraints has also been applied to control of mobile robots operating without wheel slip [5] and with wheel slip [10-13].

In [10], a linear MPC controller was designed using a model of tire compliance and suspension roll compliance to concurrently improve rollover stability and directional response, though path tracking was not considered explicitly. In [11], a path tracking MPC controller with a model of tire compliance was also proposed for use in an automated agricultural tractor. In [12], a nonlinear MPC controller is used with a nonlinear tire model to model vehicle maneuvers near the limit of friction. Due to the computational intensity of MPC, the controller is evaluated on icy road conditions, where the limit of friction can be reached at low speeds. In [13], computational requirements are studied for a similar icy road scenario with several MPC controllers of varying complexity.

While the effects of tire compliance and terrain slope on path tracking performance were acknowledged in [8], to the author's knowledge, no other path tracking controllers have been proposed that account for tire compliance effects and terrain slope. Furthermore, no path tracking controller is known to track maneuvers in excess of 0.15 g on sloped terrain.

In this paper, the MPC framework is used to design path tracking controllers based on three models of linear vehicle dynamics. It is assumed that knowledge of the environment, measurement of vehicle dynamic states, and a planned path are available. Simulation results of path tracking performance on flat ground and a sloped road departure scenario are presented for each controller. The performance of each model-based controller and the effect of slope on path tracking performance are discussed.

Manuscript received July 1, 2008.

Steven C. Peters and Karl Iagnemma are with the Department of Mechanical Engineering at the Massachusetts Institute of Technology, Cambridge, MA 02139 USA (phone: 617-452-3262, email: {scpeters | kdi}@mit.edu).

II. VEHICLE DYNAMIC MODELS

A. Kinematic bicycle model

The first model under consideration is a planar kinematic bicycle model illustrated in Fig. 1. The model assumes that the wheels roll without slipping longitudinally or laterally. States of the vehicle c.g. include position $[x_o, y_o]$, speed V , and angle ψ . The no-slip assumption implies that the velocity vector is always aligned with the vehicle's longitudinal axis. The equations of motion at constant speed for this system are:

$$\dot{x}_o = V \cos \psi \quad (1)$$

$$\dot{y}_o = V \sin \psi \quad (2)$$

$$\dot{\psi} = \frac{V}{x_f + x_r} \tan \delta \quad (3)$$

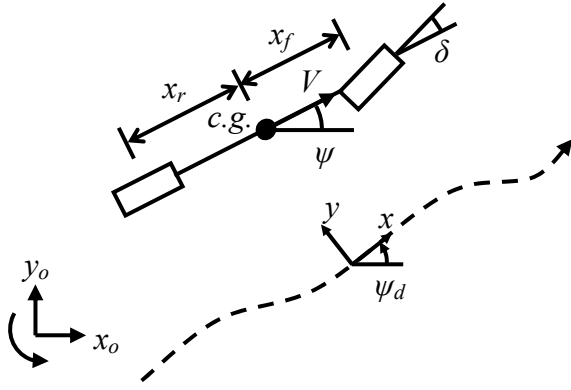


Fig. 1. Kinematic bicycle model, top view.

This is the simplest of the three models, yet it contains nonlinear terms. To be used with linear MPC methods, the model must be linearized. A reference path is defined by velocity angle ψ_d as a function of distance traveled s , which is invariant to changes in vehicle speed. Curvature of the reference path can be computed as:

$$\kappa = \frac{d\psi_d(s)}{ds} \quad (4)$$

An additional state, y , is defined that corresponds to lateral path deviation. The linearized equations of motion at constant speed are:

$$\dot{y} = V(\psi - \psi_d) \quad (5)$$

$$\dot{\psi} = \frac{V}{x_f + x_r} \delta \quad (6)$$

B. Tire compliance model

The second model under consideration includes the effect of tire compliance, relaxing the no-slip assumption to allow lateral sideslip at the wheels. As in [6,7], the lateral force acting on the tire is a function of the sideslip angle α , illustrated in Fig. 2. With a lateral stiffness coefficient of C , the force is given by

$$F_y = C\alpha \quad (7)$$

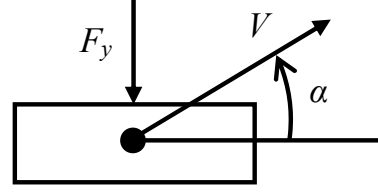


Fig. 2. Tire compliance model with velocity V , slip angle α , and lateral force F_y .

The consideration of tire compliance requires the inclusion of additional states for the velocity sideslip angle β and yaw rate $\dot{\psi}$ as illustrated in Fig. 3. In addition to the nonlinear kinematics (1) and (2), equations of motion for the vehicle are derived from momentum relations:

$$mV(\dot{\beta} + \dot{\psi}) = \sum F_y \quad (8)$$

$$I_{zz}\dot{\psi} = \sum M_z \quad (9)$$

where m is the vehicle mass and I_{zz} is the yaw moment of inertia.

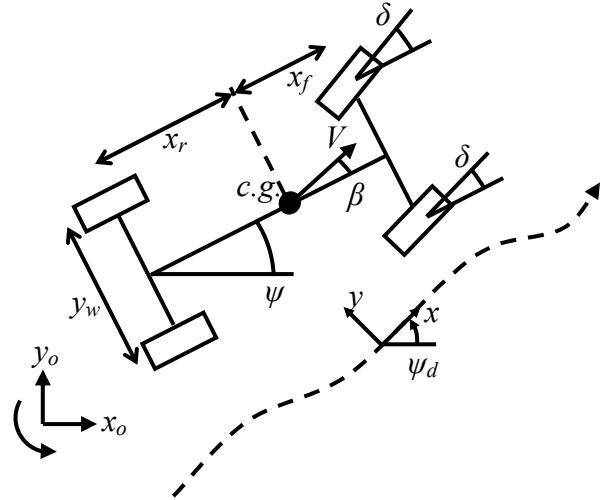


Fig. 3. Sideslip model with tire compliance, top view.

In addition to forces from tire compliance, contact forces on inclined terrain have components acting laterally to the vehicle. If the terrain elevation is a continuous, differentiable function of planar position $z(x, y)$, the terrain disturbance force T_i acting at each wheel $i=1..4$ is:

$$T_i = N_i \left(-\sin \psi \frac{\partial z}{\partial x_o} + \cos \psi \frac{\partial z}{\partial y_o} \right) \quad (10)$$

where N_i is the normal contact force at wheel i and the gradients of $z(x, y)$ are evaluated in the inertial frame.

By linearizing about the reference path as in the previous model, equations of motion are found:

$$\dot{\beta} = -\frac{C}{mV} \beta + \left(-1 + \frac{K}{mV^2}\right) \dot{\psi} + \frac{C_f}{mV} \delta + \frac{1}{mV} \sum_{i=1}^4 T_i \quad (11)$$

$$\dot{\psi} = \frac{K}{I_{zz}} \beta - \frac{D}{I_{zz}V} \dot{\psi} + \frac{C_f x_f}{I_{zz}} \delta + \frac{1}{I_{zz}} \sum_{i=1}^4 T_i x_i \quad (12)$$

$$\dot{y} = V(\psi + \beta - \psi_d) \quad (13)$$

where C_f and C_r are the cornering stiffnesses of the lumped

front wheels and lumped rear wheels, $C = C_f + C_r$, $K = C_r x_r - C_f x_f$, $D = C_f x_f^2 + C_r x_r^2$, and x_i is the longitudinal position of the i^{th} wheel relative to the c.g.

C. Suspension compliance model

The third model under consideration includes the effect of suspension compliance in addition to tire compliance. The vehicle is modeled as three rigid bodies corresponding to the chassis and front and rear axles. The vehicle suspension is modeled as revolute joints along the longitudinal axis at each axle. A single axle is illustrated in Fig. 4. In addition to the sideslip and yaw rate states, this model includes states for the body roll angle φ and body roll rate $\dot{\varphi}$.

The governing momentum relations for this model are:

$$mV(\dot{\beta} + \dot{\psi}) - m_s h \dot{\varphi} = \sum F_y \quad (14)$$

$$I_{xx} \ddot{\varphi} = \sum M_x \quad (15)$$

$$I_{zz} \ddot{\psi} = \sum M_z \quad (16)$$

where m_s is the mass of the chassis, I_{xx} is the roll moment inertia of the chassis, and h is the height of the chassis c.g. above the axle.

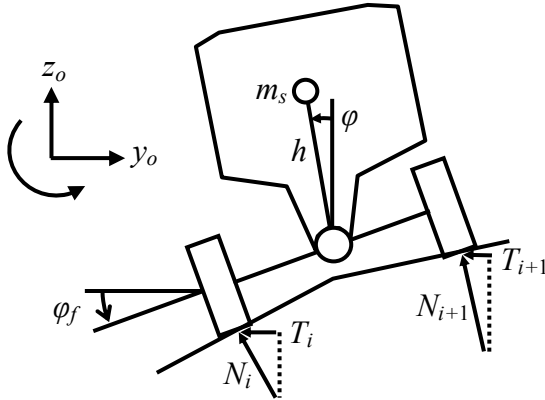


Fig. 4. Suspension compliance model, front view.

In addition to lateral force disturbances, traversing sloped terrain surfaces causes roll disturbances. The suspension moments on sloped terrain are

$$M_s = -k_f(\varphi - \varphi_f) - k_r(\varphi - \varphi_r) - b_f(\dot{\varphi} - \dot{\varphi}_f) - b_r(\dot{\varphi} - \dot{\varphi}_r) \quad (17)$$

where k_f and k_r are the stiffnesses and b_f and b_r are the damping rates of the front and rear axles and φ_f and φ_r are the terrain roll disturbances.

To compute the terrain disturbances, it is assumed that wheels always stay in contact with the terrain. Then with knowledge of the position and velocity of each wheel and the terrain elevation $z(x,y)$ the disturbances are

$$\varphi_i = \frac{z_{i+1} - z_i}{y_w} \quad (18)$$

$$\dot{\varphi}_i = \frac{\dot{z}_{i+1} - \dot{z}_i}{y_w} \quad (19)$$

where the elevation changes can be computed with

$$\dot{z}_i = \frac{\partial z}{\partial x_o} V \cos(\psi + \beta) + \frac{\partial z}{\partial y_o} V \sin(\psi + \beta) \quad (20)$$

The linearized equations of motion are then

$$\dot{\beta} = -\frac{GC}{mV} \beta + (-1 + \frac{GK}{mV^2}) \dot{\psi} + \frac{GC_f}{mV} \delta + \quad (21)$$

$$\frac{G}{mV} \sum_{i=1}^4 T_i + \frac{m_s g h^2}{VI_{xx}} \varphi + \frac{h}{VI_{xx}} M_s \quad (22)$$

$$\dot{\varphi} = \frac{m_s g h}{I_{xx}} \varphi + \frac{M_s}{I_{xx}} - \frac{Ch}{I_{xx}} \beta + \frac{Kh}{VI_{xx}} \dot{\psi} + \frac{C_f h}{I_{xx}} \delta + \frac{h}{I_{xx}} \sum_{i=1}^4 T_i$$

$$\dot{\psi} = \frac{K}{I_{zz}} \beta - \frac{D}{I_{zz} V} \dot{\psi} + \frac{C_f x_f}{I_{zz}} \delta + \frac{1}{I_{zz}} \sum_{i=1}^4 T_i x_i \quad (23)$$

$$\dot{y} = V(\psi + \beta - \psi_d) \quad (24)$$

where g is gravitational acceleration and $G = 1 + m_s h^2 / I_{xx}$.

III. MODEL PREDICTIVE CONTROL PROBLEM STATEMENT

A. Model Predictive Control Overview

Model predictive control (MPC), also known as receding horizon control, uses a system model with optimization to determine control inputs that minimize a performance objective and satisfy inequality constraints. MPC was developed in the process control industry [14]. A brief formulation of the MPC problem is provided here.

A system with linear time-invariant dynamics and discrete sampling time t_s is described by

$$\mathbf{x}_{i+1} = \mathbf{A} \mathbf{x}_i + \mathbf{B}_u \mathbf{u}_i + \mathbf{B}_v \mathbf{v}_i \quad (25)$$

$$\mathbf{y}_i = \mathbf{C} \mathbf{x}_i + \mathbf{D}_v \mathbf{v}_i \quad (26)$$

where \mathbf{u} , \mathbf{v} , \mathbf{x} , and \mathbf{y} represent the inputs, disturbances, states, and outputs of the system, respectively.

Performance objectives are specified through an objective function that is minimized and inequality constraints on the inputs and outputs. For flexibility in specifying the objective function and constraints, the input \mathbf{u}_i is defined as a cumulative sum of changes in input as in

$$\mathbf{u}_i = \mathbf{u}_{i-1} + \Delta \mathbf{u}_i \quad (27)$$

$$\mathbf{u}_{i+k} = \mathbf{u}_{i-1} + \sum_{j=0}^k \Delta \mathbf{u}_{i+j} \quad (28)$$

A prediction horizon is defined as p sampling intervals. A quadratic objective function is defined as

$$J_k = \sum_{i=k+1}^{k+p} \frac{1}{2} \mathbf{y}_i^T \mathbf{R}_y \mathbf{y}_i + \sum_{i=k}^{k+p-1} \frac{1}{2} \mathbf{u}_i^T \mathbf{R}_u \mathbf{u}_i + \sum_{i=k}^{k+p-1} \frac{1}{2} \Delta \mathbf{u}_i^T \mathbf{R}_{\Delta u} \Delta \mathbf{u}_i \quad (29)$$

Inequality constraints are defined as

$$\mathbf{y}_{\min} \leq \mathbf{y}_i \leq \mathbf{y}_{\max} \quad (30)$$

$$\mathbf{u}_{\min} \leq \mathbf{u}_i \leq \mathbf{u}_{\max}$$

$$\Delta \mathbf{u}_{\min} \leq \Delta \mathbf{u}_i \leq \Delta \mathbf{u}_{\max}$$

The vectors \mathbf{y} , \mathbf{u} , $\Delta \mathbf{u}$, and \mathbf{v} over the prediction horizon are augmented into vectors \mathbf{Y} , \mathbf{U} , $\Delta \mathbf{U}$, and \mathbf{V} as in

$$\mathbf{Y}_{k+1} = \begin{bmatrix} \mathbf{y}_{k+1} \\ \mathbf{y}_{k+2} \\ \dots \\ \mathbf{y}_{k+p} \end{bmatrix}, \mathbf{U}_k = \begin{bmatrix} \mathbf{u}_k \\ \mathbf{u}_{k+1} \\ \dots \\ \mathbf{u}_{k+p-1} \end{bmatrix}, \Delta \mathbf{U}_k = \begin{bmatrix} \Delta \mathbf{u}_k \\ \Delta \mathbf{u}_{k+1} \\ \dots \\ \Delta \mathbf{u}_{k+p-1} \end{bmatrix}, \mathbf{V}_k = \begin{bmatrix} \mathbf{v}_k \\ \mathbf{v}_{k+1} \\ \dots \\ \mathbf{v}_{k+p-1} \end{bmatrix} \quad (31)$$

The matrices \mathbf{S}_u , \mathbf{S}_{u1} , \mathbf{S}_x , and \mathbf{H}_x can then be found to compute the augmented outputs from inputs and disturbances as in

$$\mathbf{Y}_{k+1} = \mathbf{S}_x \mathbf{x}_k + \mathbf{S}_{u1} \mathbf{u}_{k-1} + \mathbf{S}_u \Delta \mathbf{U}_k + \mathbf{H}_v \mathbf{V}_k \quad (32)$$

Likewise, the matrices \mathbf{H} , \mathbf{F}_x , \mathbf{F}_u , and \mathbf{F}_v can be found to express the objective function in terms of the augmented vectors with constant terms removed, which is given as

$$J_k = \frac{1}{2} \Delta \mathbf{U}_k^T \mathbf{H} \Delta \mathbf{U}_k + (\mathbf{x}_k^T \mathbf{F}_x + \mathbf{u}_{k-1}^T \mathbf{F}_u + \mathbf{V}_k^T \mathbf{F}_v) \Delta \mathbf{U}_k \quad (33)$$

Finally, the matrices \mathbf{A}_c and \mathbf{b}_c can be expressed in matrix form as

$$\mathbf{A}_c \Delta \mathbf{U}_k \leq \mathbf{b}_c \quad (34)$$

The MPC control problem is now expressed as a quadratic program that can be solved with conventional optimization routines. For further details of the MPC problem setup, the reader is referred to the relevant literature [14, 15].

B. Path tracking MPC problem

In this section, path tracking controllers are presented in the MPC framework for each model specified in Section II. For each model, the only component of the output vector \mathbf{y} is the state y corresponding to lateral path deviation. The objective function J is then defined as

$$J_k = \sum_{i=k+1}^{k+p} \frac{1}{2} R_y y_i^2 + \sum_{i=k}^{k+p-1} \frac{1}{2} R_{\Delta\delta} \Delta\delta_i^2 \quad (35)$$

where R_y is the weight on path tracking error and $R_{\Delta\delta}$ is an input weight required for convergence of the optimization routine. For this paper, values of $R_y = 10$ and $R_{\Delta\delta} = 0.01$ were used.

It is assumed that the magnitude and rate of steering inputs is constrained as

$$-\delta_{\max} \leq \delta_i \leq \delta_{\max} \quad (36)$$

$$-\dot{\delta}_{\max} t_s \leq \Delta\delta_i \leq \dot{\delta}_{\max} t_s \quad (37)$$

where δ_{\max} is the maximum steering angle and $\dot{\delta}_{\max}$ is the maximum steering rate. Human drivers are reported to be capable of turning the steering wheel at 1000 deg/s [16], which corresponds to a steering rate of 30 deg/s at the tires for a typical steering ratio. Thus for this paper, values of $\delta_{\max} = 20$ deg and $\dot{\delta}_{\max} = 30$ deg/s were used.

Other performance specifications, such as limits on sideslip angle or body roll angle can easily be included in this framework [10], but are not considered here.

As mentioned in the previous section, the MPC framework has the capacity for incorporating knowledge of future disturbances into the controller optimization if such knowledge is available. Since terrain disturbances are a function of terrain elevation $z(x,y)$, a prediction of the robot's path is needed to estimate the future disturbances.

TABLE I
ADAMS MODEL PARAMETERS

Symbol	Description	Value
x_f	c.g. position	1.13 m
x_r	c.g. position	1.43 m
y_w	vehicle width	1.56 m
m	total vehicle mass	2030 kg
m_s	chassis sprung mass	1880 kg
I_{xx}	roll moment of inertia	834 kg m ²
I_{zz}	yaw moment of inertia	3050 kg m ²
h	sprung c.g. height	0.34 m
C_f	front cornering stiffness	94000 N / rad
C_r	rear cornering stiffness	65300 N / rad
k_f	front axle roll stiffness	30e3 Nm / rad
k_r	rear axle roll stiffness	30e3 Nm / rad
b_f	front axle roll damping	1600 Nms / rad
b_r	rear axle roll damping	1600 Nms / rad

Since the MPC controller predicts a trajectory along with control inputs, the trajectory from the previous control computation is used to compute terrain disturbances. If the knowledge of disturbances is not available, the disturbance rejection properties of the controller will determine performance.

C. Simulation results

In this section simulation results are presented to demonstrate the performance of this control method. A model of a generic, high-centered light truck was developed in the commercial multibody dynamic simulation software package ADAMS. The vehicle features a double wishbone suspension, rack and pinion steering, and a V8 engine. Critical vehicle parameters are listed in Table 1.

The aggressive maneuver chosen for these tests was the double lane change maneuver, illustrated in Fig. 6. The curvature and heading angles are also shown. The curvature changes rapidly in this maneuver, indicating that vehicle dynamics may be excited. The aggressiveness of the maneuver is adjusted by choosing a lateral acceleration a_y in g's and speed V and computing the appropriate curvature magnitude with

$$\kappa = \frac{a_y g}{V^2} \quad (38)$$

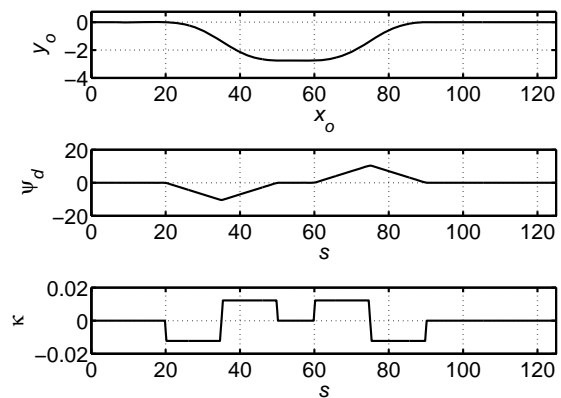


Fig. 6. Reference trajectory, from top to bottom: path (m), heading angle (deg), and curvature (1/m). Both heading angle and curvature are plotted against distance traveled s (m).

Simulations of the MPC controllers designed for each model were conducted at 20 m/s (45 mph) with lateral acceleration of 0.5 g on flat ground with friction coefficient of 1.0. A prediction horizon of 1.5 s with MPC sampling time of 0.03 s was used. The path taken by each controller is shown in Fig. 7(a) and the path tracking error in Fig. 7(b). The maximum and root-mean square path tracking error is given in Table II. It can be seen that both controllers with models of vehicle compliance perform better than the kinematic model.

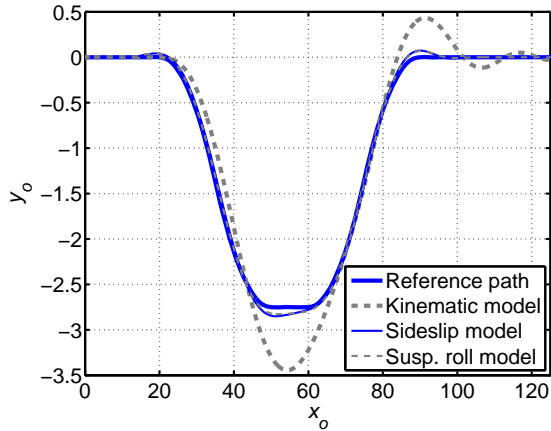


Fig. 7(a). Simulated double lane change maneuvers on flat ground. “Kinematic model” is the controller with kinematic bicycle model, “Sideslip model” is the controller with tire compliance model, and “Susp. roll model” is the controller with tire and suspension compliance model.

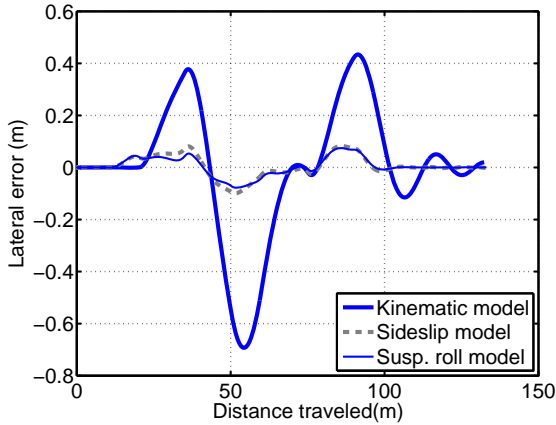


Fig. 7(b). Lateral path error in flat ground simulations.

TABLE II
PATH TRACKING ERROR ON FLAT GROUND

Model	Maximum error	Root-mean square error
Kinematic	0.69 m	0.25 m
Tire compliance	0.10 m	0.04 m
Tire/suspension compliance	0.08 m	0.03 m

In addition to the on-road scenario, a road departure simulation was also conducted on a road surface with sloped shoulders. A cross section of the road departure terrain can be seen in Fig. 8. All portions of the terrain were modeled as rigid surfaces with a friction coefficient of 1.0.

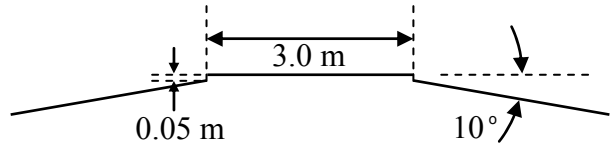


Fig. 8. Cross section of road departure terrain.

Simulations of each controller with the same conditions as before were conducted on the road departure terrain. Although the reference path completely departs and reenters the road surface, the terrain surface was assumed to be flat by the controllers. The path tracking performance is shown in Fig. 9(a)-(b) and summarized in Table III. The models with compliance again perform much better than the kinematic model, though disturbances from terrain slope degrade path tracking performance from that on flat ground.

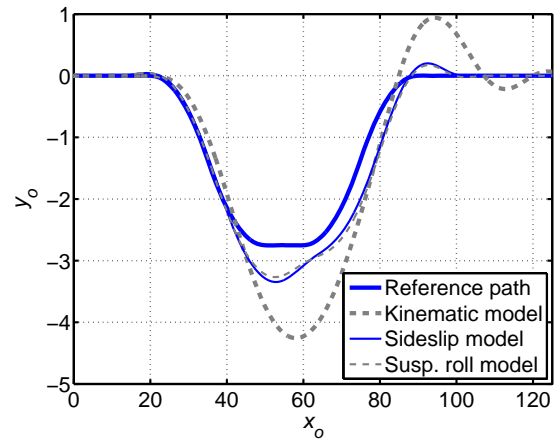


Fig. 9(a). Simulated double lane change maneuvers on road departure terrain.

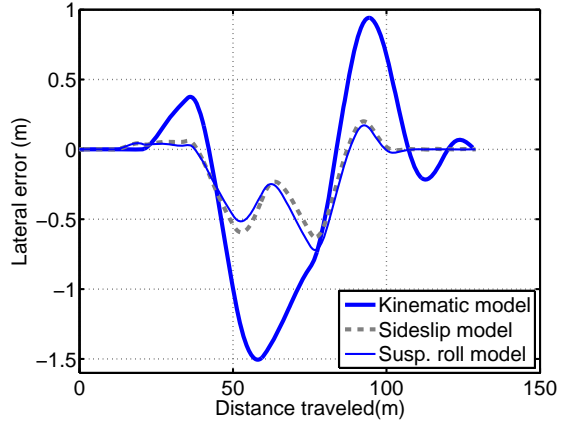


Fig. 9(b). Lateral path error in road departure simulations.

TABLE III
PATH TRACKING ERROR ROAD DEPARTURE

Model	Maximum error	Root-mean square error
Kinematic	1.51 m	0.66 m
Tire compliance	0.63 m	0.26 m
Tire/suspension compliance	0.72 m	0.27 m

Simulations were also performed on the road departure terrain with knowledge of terrain elevation available to the

controllers. The predicted paths are used with the relations described in Section II to estimate the disturbances caused by terrain slope. The effect of advance terrain knowledge on path tracking error is shown in Fig. 10(a) for the tire compliance model and Fig. 10(b) for the suspension compliance model. The maximum and root-mean square of path tracking error are given in Table IV. No comparison is shown for the kinematic model since it does not consider the effect of slopes.

TABLE IV
PATH TRACKING ERROR ROAD DEPARTURE

Model		Maximum error	Root-mean square error
Tire compliance	Slope unaware	0.63 m	0.26 m
	Slope aware	0.50 m	0.19 m
Tire/susp. compliance	Slope unaware	0.72 m	0.27 m
	Slope aware	0.56 m	0.19 m

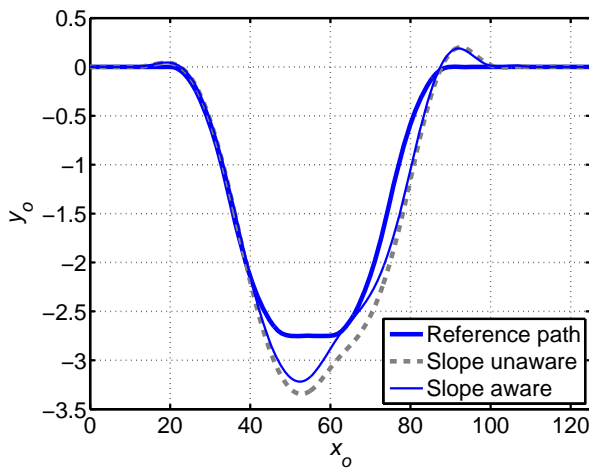


Fig. 10(a). Tire compliance model predictive controller with and without knowledge of terrain slopes.

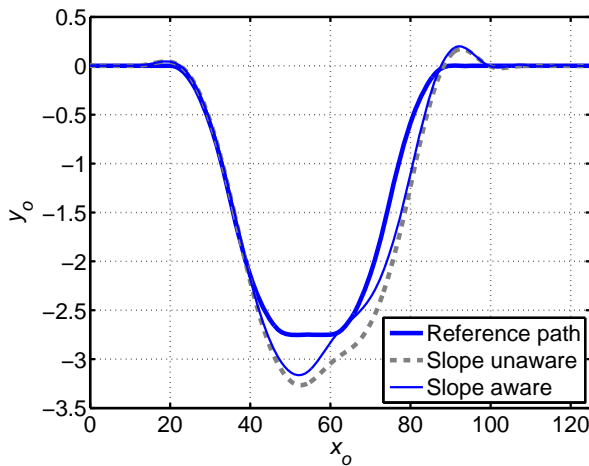


Fig. 10(b). Tire and suspension compliance model predictive controller with and without knowledge of terrain slopes.

It can be seen that advance knowledge of terrain disturbances reduces path tracking error measurably, though performance is still worse than on flat ground. This may be caused by nonlinearities not captured in the linear model such as intermittent loss of ground contact during road departure. Future work will seek to determine the effects

impeding improved path tracking performance on sloped terrain.

IV. CONCLUSION

Path tracking controllers based on three linear models of vehicle dynamics are presented in the MPC framework. Lateral path tracking error is computed in high-fidelity ADAMS simulations for an aggressive double lane change maneuver on flat ground and in road departure. Controllers that consider tire compliance perform much better than the kinematic model predictive controller. Advance knowledge of terrain disturbances is shown to measurably improve path tracking performance in road departure situations.

REFERENCES

- [1] Buehler, M., Iagnemma, K., and Singh, S., (eds.) *The 2005 DARPA Grand Challenge: The Great Robot Race*, Springer Tracts in Advanced Robotics (STAR) Series, v. 36, Springer, August, 2007.
- [2] National Highway Traffic Safety Administration, DOT HS 809 919, *Traffic Safety Facts 2004: A Compilation of Motor Vehicle Crash Data from the Fatality Analysis Reporting System and the General Estimates System*, USA, 2006.
- [3] Y. Kanayama, Y. Kimura, F. Miyazaki and T. Noguchi, "A stable tracking control method for an autonomous mobile robot," *Proc. 1990 IEEE Intl. Conf. Robotics and Automation*, pp. 384-389, 1990.
- [4] C. C. de Wit and O. J. Sordalen, "Exponential stabilization of mobile robots with nonholonomic constraints," *IEEE Trans. Automatic Control*, v. 37, n. 11, pp. 1791-1797, 1992.
- [5] G. Klancar and I. Skrjanc, "Tracking-error model-based predictive control for mobile robots in real time," *Robotics and Autonomous Systems*, v. 55, n. 6, pp. 460-469, 2007.
- [6] H. B. Pacejka, *Tire and Vehicle Dynamics* (2nd ed.), Warrendale, PA: Society of Automotive Engineers, 2006.
- [7] L. Segel, "Theoretical Prediction and Experimental Substantiation of the Response of the Automobile to Steering Control," *Proc. of Automotive Division, Inst. Mech. Engineers, London*, pp. 310-330, 1956-1957.
- [8] H. Peng and M. Tomizuka, "Preview Control for Vehicle Lateral Guidance in Highway Automation," *Journal of Dynamic Systems, Measurement, and Control*, v. 115, pp. 679-686, December 1993.
- [9] A. Alleyne, "Comparison of alternative obstacle avoidance strategies for vehicle control," *Vehicle System Dynamics*, v. 27, n. 5-6, pp. 371-392, June 1997.
- [10] C. R. Carlson and C. J. Gerdes, "Optimal rollover prevention with steer by wire and differential braking," *Proc. ASME Dynamic Systems and Control Division - 2003*, pp. 345-354, November 2003.
- [11] R. Lenain, B. Thuilot, C. Cariou and P. Martinet, "Model Predictive Control for Vehicle Guidance in Presence of Sliding: Application to Farm Vehicles Path Tracking," *Proc. 2005 IEEE Intl. Conf. Robotics and Automation*, pp. 885-890, 2005.
- [12] P. Falcone, F. Borrelli, J. Asgari, H. E. Tseng, D. Hrovat, "Predictive Active Steering Control for Autonomous Vehicle Systems," *IEEE Trans. Control Systems Technology*, v. 15, n. 3, pp. 566-580, 2007.
- [13] T. Besselmann, P. Rostalski, M. Morari, "Hybrid Parameter-Varying Model Predictive Control for Lateral Vehicle Stabilization," *Proc. European Control Conference*, July 2007.
- [14] C. E. Garcia, D. M. Prett and M. Morari, "Model predictive control: theory and practice - a survey," *Automatica*, v. 25, n. 3, pp. 335-348, 1989.
- [15] A. Bemporad, M. Morari and N. L. Ricker, *Model Predictive Control Toolbox 2: User's Guide*, The Mathworks, Inc., Natick, MA, 2007.
- [16] A. Hac, "Rollover Stability Index Including Effects of Suspension Design," *SAE Transactions*, n. 2002-01-0965, 2002.